Author(s): Hänninen, Mikko M.; Paturi, Petriina; Tuononen, Heikki; Sillanpää, Reijo; Lehtonen, Ari

Title: Heptacoordinated Molybdenum(VI) Complexes of Phenylenediamine Bis(phenolate): A Stable Molybdenum Amidophenoxide Radical

Year: 2013

Version:

Please cite the original version:

Hänninen, M. M., Paturi, P., Tuononen, H., Sillanpää, R., & Lehtonen, A. (2013). Heptacoordinated Molybdenum(VI) Complexes of Phenylenediamine Bis(phenolate): A Stable Molybdenum Amidophenoxide Radical. Inorganic Chemistry, 52(10), 5714-5721. https://doi.org/10.1021/ic302355b

Heptacoordinated Molybdenum(VI) Complexes of Phenylenediamine Bis(phenolate): A Stable Molybdenum-Amidophenoxide Radical

*Mikko M. Hänninen,[†] Petriina Paturi,[‡] Heikki M. Tuononen,[†] Reijo Sillanpää,[†] and Ari Lehtonen[§]**

[†]Department of Chemistry, P.O. Box 35, University of Jyväskylä, FI-40014 Jyväskylä, Finland

[‡]Wihuri Physical Laboratory, Department of Physics and Astronomy, University of Turku, FI-20014, Turku, Finland

[§]Department of Chemistry, University of Turku, FI-20014, Turku, Finland

KEYWORDS

non-innocent ligands, molybdenum complex, amidophenoxide radical, DFT calculations, electronic structure

ABSTRACT

The syntheses, crystallographic structures, magnetic properties and theoretical studies of two heptacoordinated molybdenum complexes with N,N'-bis(3,5-di-*tert*-butyl-2-hydroxyphenyl)-1,2-phenylenediamine ($H_4N_2O_2$) are reported. A formally Mo(VI) complex **1** [$Mo(N_2O_2)Cl_2(dmf)$] was synthesized by the reaction between [$MoO_2Cl_2(dmf)_2$] and $H_4N_2O_2$, whereas the other Mo(VI) complex **2** [$Mo(N_2O_2)(HN_2O_2)$] was formed when [$MoO_2(acac)_2$] was used as a molybdenum source. Both complexes represent a rare case of Mo(VI) ion without any multiply bonded terminal ligands. In addition, molecular structure, magnetic measurements, ESR spectroscopy and density functional theory calculations indicate that the complex **2** is the first stable Mo(VI)-amidophenoxide radical.

INTRODUCTION

Redox-active catechols and *ortho*-aminophenols are of great interest as non-innocent ligands for their ability to contribute to electronic properties typically associated with metal valence electrons.[1] One example of such ligands is N,N'-bis(3,5-di-*tert*-butyl-2-hydroxyphenyl)-1,2-phenylenediamine ($H_4N_2O_2$) that can be viewed as a dimeric derivative of two bidentate *ortho*-aminophenols.[2] Thus, it can act, once partially or fully deprotonated, as a multidentate ligand to form complexes with Cu and Zn[2] as well as with Ti and Zr.[3,4] This potentially tetradentate ligand has rich electrochemical behavior and it can present five different oxidation states that are interrelated by one-electron transfer steps (see

Chart **1**).

Oxomolybdenum(VI) complexes of various multidentate nitrogen based ligands are known to behave as active catalysts in bioinspired oxotransfer reactions.[5,6,7] In the current contribution, we

wanted to combine the redox-active nature of the ligand $H_4N_2O_2$ with the reactive MoO_2 functionality to generate new potential oxotransfer catalysts. However, in our experiments the reaction of $H_4N_2O_2$ with several MoO_2^{2+} sources did not yield the desired oxomolybdenum(VI) complex because the terminal oxo groups of the molybdenyl ion were removed upon ligand coordination. In the present paper, we report the syntheses, molecular structures and magnetic behavior of two new molybdenum complexes with the N_2O_2 ligand. The synthesized heptacoordinated complexes $[Mo(N_2O_2)Cl_2(dmf)]$ (**1**) and $[Mo(N_2O_2)(HN_2O_2)]$ (**2**) are of interest due to their general coordination chemistry and the non-innocent behavior of the ligand. In support of the experimental work, we also carried out a comprehensive computational study to address the electronic nature of compounds **1** and **2**.

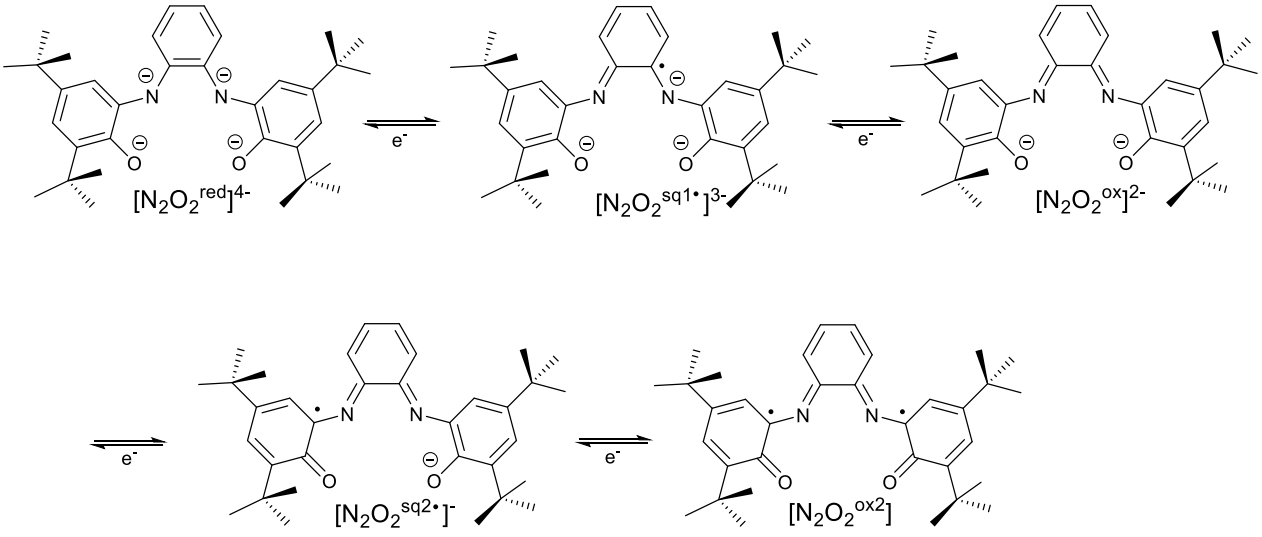

Chart 1. Different oxidation states of the deprotonated ligand N_2O_2. Adapted from Ref. 2

RESULTS AND DISCUSSION

Synthesis of [Mo(N_2O_2)Cl_2(dmf)] 1.

The stoichiometric reaction of [$MoO_2Cl_2(dmf)_2$] with $H_4N_2O_2$ in methanol or acetonitrile lead to a rapid formation of an intensely colored solution that afforded dark green shiny air-stable crystals in high yield (Scheme 1). The crystals are practically insoluble in common organic solvents or water, which prevents any NMR analyses. The infrared spectrum of the compound lacks the bands characteristic of a Mo=O function, which indicates the loss of molybdenyl oxo groups during complexation. Structural analysis by X-ray crystallography (see below) show that the solid state structure of compound **1** consists of separated neutral molecules of [Mo(N_2O_2)Cl_2(dmf)]. Thus, in the formation of complex **1**, two metal-oxo bonds have been cleaved while two metal-chloride bonds have remained intact. This result was quite unexpected although similar reactivity with MoO_2Cl_2 derivatives has been observed earlier.[8,9] In general, the cleavage of both metal-oxo bonds and the formation of a Mo(VI) compound without any multiply bonded terminal ligands is rare.[10] As structurally comparable 2,2′-biphenyl-bridged bis(2-aminophenol) ligand 4,4′-di-*tert*-butyl-*N*,*N*′-bis(3,5-di-*tert*-butyl-2-hydroxyphenyl)-2,2′-diaminobiphenyl (H_4^{t}BuClip) is reported to react with $MoO_2(acac)_2$ to form [MoO_2(H_2^{t}BuClip)] where the diarylamines remain protonated and bind trans to the terminal oxo groups.[10] In our studies, the elimination of both oxo moieties is probably due to the rigid geometry of the ligand system, which precludes the formation of the favorable *cis*-MoO_2 structure. This and the relatively vague geometrical parameters of the product inspired us to study the bonding in detail (see below).

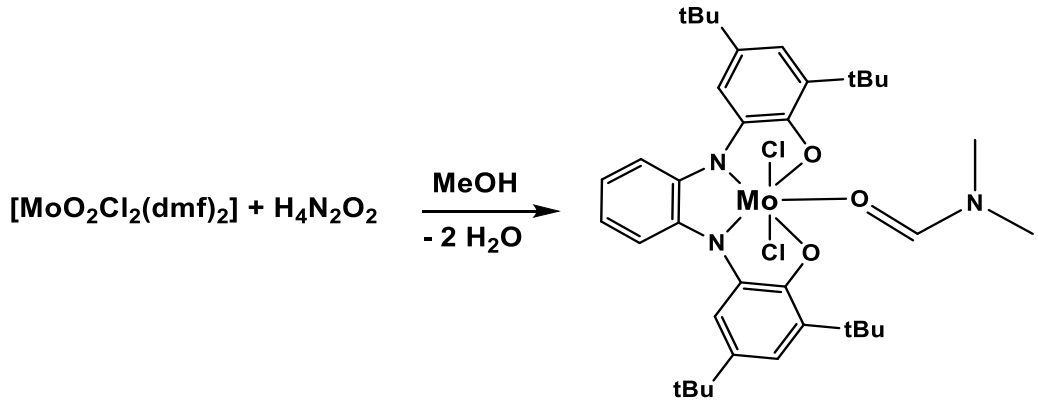

Scheme 1. Formation of [Mo(N_2O_2)Cl_2(dmf)] **1**.

Synthesis of [Mo(N_2O_2)(HN_2O_2)] 2.

When [MoO_2(acac)$_2$] was reacted with $H_4N_2O_2$ in methanol, a dark solution was formed upon which black shiny air-stable crystal of **2** deposited at ambient temperature. The compound is soluble in hydrocarbon solvents and ethers, but virtually insoluble in methanol. The reaction was repeated in different stoichiometries to have identical product in lower yields without any sign of a 1:1 complex. Similar crystals were obtained using the structurally analogous [MoO_2(Heg)$_2$] (Heg^- = ethanediolate monoanion) as a starting material. The ^{1}H NMR spectrum of **2** does not offer any structural information as it shows only broad overlapping signals for the *tert*-butyl groups as well as for the hydrogen atoms in the aromatic rings. Similarly to **1**, the infrared spectrum of **2** does not display any characteristic absorption for the Mo=O moiety. The structure of the compound was verified by X-ray crystallography (see below) to be a neutral molybdenum complex where two different ligands are coordinated to the metal. The protonation states of the ligands were verified by the observation of a peak in the electrospray mass spectrum at the mass expected for the empirical formula. Interestingly, both ESI(+) and ESI(-) mode gave similar peak patterns with the characteristic isotope distribution of the metal. It seems that the molecular

cation is formed due to the removal of the odd electron, whereas the molecular anion is formed by the reduction of the metal or pairing of the odd electron.

Analytical samples of **2** were obtained from freshly prepared reaction mixtures as the material seems to metamorphose upon standing for a longer period of time. Although the physical appearance and unit cell parameters of the crystals remain unchanged over time, their diffraction intensities decrease significantly. This causes the refinement of the structure to fail due to the strong disorder of the ring atoms, which in turn suggests that the oxidation state of the ligand and/or metal can vary without any substantial changes in the overall molecular structure.

The cyclic voltammogram of **2** was measured in acetonitrile in the potential range from +2.0 to -1.7 V vs. Fc^{+}/Fc. Three distinct one-electron oxidation waves (+0.41, +0.83 and +1.23 V) and three one-electron reduction waves (-0.01, -0.63 and -1.26 V) are seen within the solvent window (see Supporting Information). For comparison, the ligand-based redox potentials for $[Zn(N_2O_2^{ox})]$ are seen at +0.03 and +0.37 V for oxidation and at -0.64 and -1.29 V for reduction, respectively.

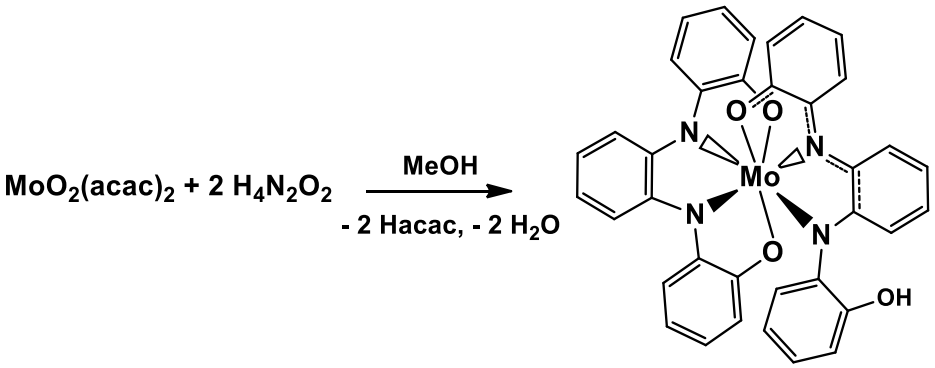

Scheme 2. Formation of $[Mo(N_2O_2)(HN_2O_2)]$ **2**. The *tert*-butyl groups of the ligand N_2O_2 are omitted for clarity.

STRUCTURAL STUDIES

Crystals of **1** were obtained from the reaction mixture in acetonitrile. In the solid state structure (Figure 1), the molybdenum atom shares a plane with two oxygen atoms and two nitrogen atoms from the N_2O_2 ligand as well as with one oxygen donor from the coordinated dmf ligand. Two chlorides in axial positions complete the heptacoordinated environment around the metal center which is best described as a distorted pentagonal bipyramid.[11] In principle, the protonation and oxidation level of the $H_4N_2O_2$ ligand can be determined from high quality single crystal X-ray data as the C-C, C-N and C-O distances change systematically upon stepwise one-electron oxidation processes.1 In **1**, the C-C bond lengths within both the phenolic parts of the N_2O_2 ligand and the central ring fall in the range 1.38 – 1.41 Å (Table 1), which does not allow unambiguous definition of the oxidation state of the ligand. Similarly, the C-N and C-O bond distances of 1.398 Å and 1.322 Å, respectively, indicate that the ligand oxidation state might be either -1 or -2 (Chart 1), while the observed metal to donor atom distances are characteristic for anionic phenoxide and amide ligands. Consequently, theoretical calculations at the DFT level were performed for a model system of **1** (see below).

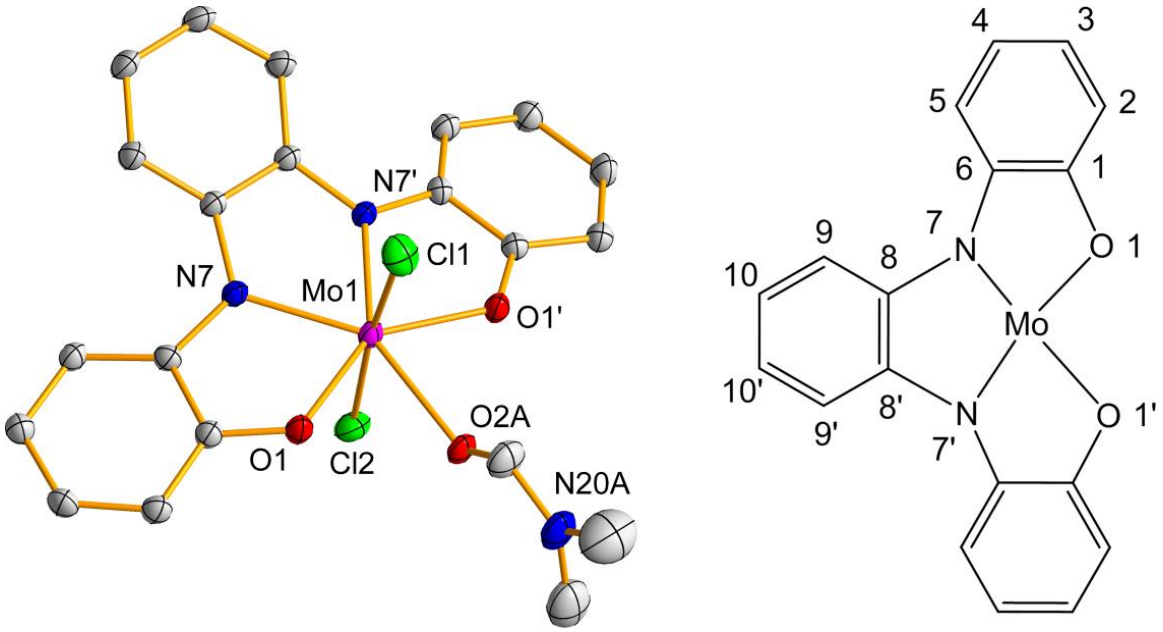

Figure 1. Crystal structure of **1** (left) and its numbering scheme (right). Symmetry operation: x, 0.5-y, z. C-H hydrogens, *tert*-butyl substituents and other parts of the disordered dmf molecule are omitted for clarity. Thermal ellipsoids are drawn at the 30% probability level.

The single crystals of **2** were separated from the methanol solution of the ligand and $[MoO_2(acac)_2]$ as described above. X-ray structure (Figure 2) showed that the asymmetric unit consists of two crystallographically independent molecules with comparable structural parameters (Table 1). In these molecules, both the oxo moieties and the acetylacetonato ligands have been replaced during complexation, the final product being a neutral heptacoordinated complex $[Mo(N_2O_2)(HN_2O_2)]$ where the ligand displays two different coordination modes. One of the two ligands is fully deprotonated, whereas the other ligand has a dangling phenol part with an intact OH group. The formal oxidation state of the Mo center can again be estimated from the oxidation levels of these two different ligands. Similarly to complex **1**, the ligand assembly is not unambiguous since the quality of the X-ray data does now allow an in-depth analysis of the geometrical parameters. Nevertheless, the tetradentate ligand seems to be analogous to a fully

deprotonated $[N_2O_2^{red}]^{4-}$ (Chart 1) as in **1**, whereas the tridentate ligand with a dangling phenol part can be best described as a triply deprotonated ligand $[HN_2O_2^{sq1\cdot}]^{2-}$ (Chart 1). With these presumptions, the formal oxidation state of the metal center is Mo(VI). As the oxidation level assumed for the tridentate ligand involves one unpaired electron, the material should be paramagnetic.

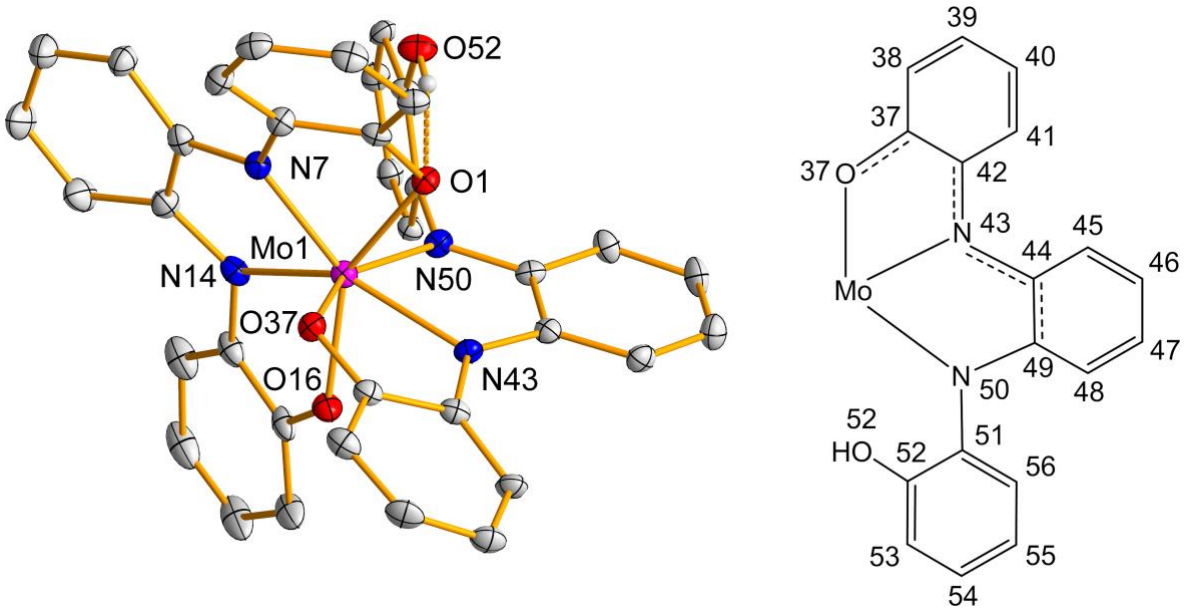

Figure 2. Crystal structure of **2** (left) and its numbering scheme (right). C-H hydrogens and *tert*-butyl substituents are omitted for clarity. Thermal ellipsoids are drawn at the 30% probability level.

MAGNETIC PROPERTIES

Compound **1** showed only a diamagnetic signal as expected due to the even number of electrons. Compound **2**, on the other hand, gave a paramagnetic signal with susceptibility χ_{mol} = 4.2×10^{-7} m^3/mol at 5 K ($\chi_{mol} = M\cdot\chi_v/\rho$, where ρ is the density, M is molar mass and χ_v is volume magnetic susceptibility). The temperature dependence of the susceptibility was also measured

and the data fitted to the Curie-law of localized moments, $\chi_{mol} = C/(T-\theta_p)$. Figure 3 shows the $\chi_{mol}T$ *vs. T* plot of **2** (bottom) as well as the plots of χ_{mol} *vs. T* and $1/\chi_{mol}$ *vs. T* (top). As can be seen from the figure, the inverse of susceptibility does not obey the Curie law, which means that the magnetic spin is not localized. However, χ_{mol} is not temperature independent either as would be expected for Pauli paramagnetism induced by a completely non-localized electron. Consequently, the most probable explanation of the data measured for compound **2** is a partially localized unpaired electron that is causing the magnetic properties.[12] The calculated magnetic moment (μ_{eff}) at the high temperature range (T > 150 K) is 1.80 B.M. whereas it is 1.25 B.M. at the low temperature range (T < 80 K). As the 'spin only' value for an unpaired electron is 1.73 B.M., the magnetic moment at the high temperature range clearly indicates the presence of only one unpaired electron.

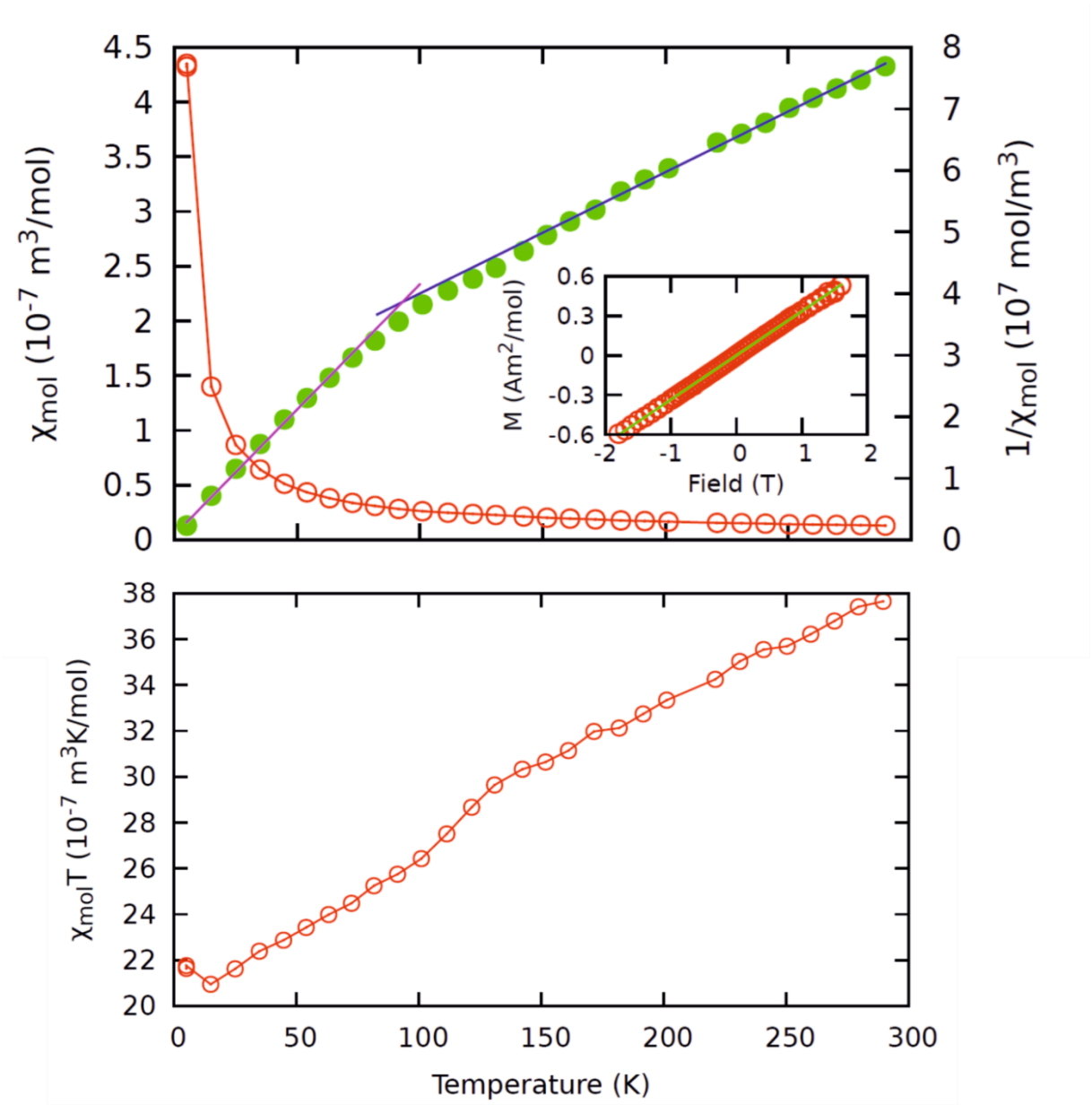

Figure 3. Plot of susceptibility χ_{mol} *vs. T* (top) and $\chi_{mol}T$ *vs. T* (bottom) of compound **2** in a 0.1 T field. The green dotted values show $1/\chi_{mol}$ with a fit to the Curie law at the high (blue line) and low temperature (violet line) regime. The inset shows the magnetic field dependence at 5 K with a linear fit giving $\chi_{mol} = 4.2\times10^{-7}$ m^3/mol.

ESR SPECTROSCOPY

X-band electron spin resonance (ESR) spectra of the solid compounds **1** and **2** were measured at room temperature as well as at 4 K, whereas the solution spectrum of **2** was measured in CH_2Cl_2 at room temperature. As expected, compound **1** did not show an ESR signal, while a solid sample of **2** gave an axial spectrum at 4 K with $g_\perp$ = 2.0157 and $g_\parallel$ = 2.0047 (see Supporting Information). Thus, the calculated Δg = 0.011 and $\langle g \rangle$ = 2.012. In CH_2Cl_2, **2** produced a nearly isotropic ESR signal (S=½) g_{iso} = 2.0087 with minor asymmetry, possibly due to an unresolved hyperfine interaction. These values clearly indicate that the unpaired electron is predominantly on the orbitals of the ligand, in a similar fashion as in Ni(II) and Ru(II) semiquinone complexes,[13] and not on the metal as $\langle g \rangle$ varies from 1.938 to 1.952 in several octahedral Mo(V) compounds.[14] Against this scenario, **2** is best described as a molybdenum(VI) complex with a semiquinone-type radical ligand.

THEORETICAL STUDIES

Since the oxidation state of the ligands in **1** and **2** cannot be explicitly determined from the X-ray diffraction data, DFT calculations were performed to shed light to the electronic structure and bonding of the ligands in these complexes. Generally in the non-innocent $C_6H_4(NR)_2$-*o* and $C_6H_4(O)(NR)$-*o* species (R = H, alkyl, aryl), the discrimination between the completely reduced amido and phenoxido or oxidized imino and quinone formulation of the ligand is done by inspecting the trends in the experimentally determined C-C, C-N and C-O bond distances, which obviously requires very high quality X-ray diffraction data.[1,15,16] In addition, the partially reduced radical *o*-benzosemiquinoneiminato form should be recognizable by comparison of these bond distances.[17] As earlier studies have shown,[18] computational analyses provide in many cases

crucial information when determining the electronic nature of the coordinating ligand and that of the entire complex, especially when the experimental structural data is inconclusive.

In order to determine the correct electronic states of the metals and ligands in both **1** and **2**, the geometries of model complexes **1'** and **2'** (*tert*-butyl substituents replaced with methyl groups) were optimized using the PBE1PBE[19] functional and def2-TZVP[20] basis sets. The nature of the stationary points found was addressed by the subsequent calculation of two of the lowest eigenvalues of the Hessian matrix. Selected geometrical parameters of the optimized structures are given in Table 1.

For **1**, there exist three plausible electronic states: a closed shell singlet **1'**-S, a high-spin triplet **1'**-T and a broken symmetry singlet diradical **1'**-DR. Geometry optimizations were performed for all of these states and the results indicate that the triplet state is about 30 kJ/mol higher in energy than either of the two singlet states (in agreement with magnetometric measurements) and therefore will not be discussed further. From the two singlet states, the ground state is the diradical state **1'**-DR which however is only 5 kJ mol^{-1} lower in energy than **1'**-S. Considering such a small energy difference between these states, the diradical nature of complex **1** is relatively small, which is also evident from the calculated frontier molecular orbitals (MOs, see below) and from the spin distribution of the broken symmetry solution (Figure). According to the Mulliken population analysis and the calculated spin density,[21] the formally unpaired electrons in **1'**-DR are localized mostly at the nitrogen atoms of the ligand and at the molybdenum center. The diamagnetism in **1'**-DR is then due to the relatively strong antiferromagnetic coupling between these electrons, which results in an S = 0 state.

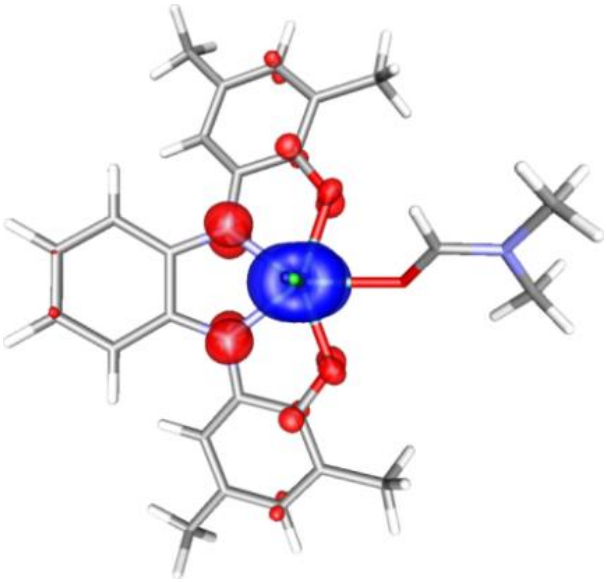

Figure 4. Calculated spin density distribution of complex **1'**-DR. Red and blue denote excess alpha and beta spin density, respectively.

Table 1. Selected geometrical parameters of **1'** and **2'** as compared with the X-ray data. (For numbering scheme, see Figures 1 and 2).

		1	**1'**-S	**1'**-DR			**2a**	**2b**	$\mathbf{2}^{AVG}$	**2'**-D
Mo	N7	2.065(2)	2.034	2.077	Mo1	N43	2.149(3)	2.152(4)	2.151	2.167
Mo	N7'	2.065(2)	2.042	2.082	Mo1	N50	2.022(3)	2.024(3)	2.023	2.026
Mo	O1	1.982(1)	1.997	1.998	Mo1	O37	2.004(3)	1.997(3)	2.001	1.989
Mo	O1'	1.982(1)	1.966	1.970	Mo1	O52	3.566(4)	3.574(4)	3.570	3.632
O1	C1	1.322(2)	1.312	1.309	O37	C37	1.324(6)	1.344(6)	1.334	1.313
N7	C6	1.398(3)	1.390	1.378	N43	C42	1.375(5)	1.377(6)	1.376	1.357
C1	C2	1.407(3)	1.398	1.400	C37	C38	1.412(6)	1.404(6)	1.408	1.403
C2	C3	1.380(3)	1.384	1.382	C38	C39	1.375(7)	1.385(7)	1.380	1.380
C3	C4	1.411(3)	1.400	1.404	C39	C40	1.415(7)	1.402(6)	1.409	1.407
C4	C5	1.376(3)	1.385	1.382	C40	C41	1.397(6)	1.388(7)	1.393	1.378
C5	C6	1.401(3)	1.396	1.399	C41	C42	1.391(7)	1.401(7)	1.396	1.406
C6	C1	1.400(3)	1.392	1.398	C37	C42	1.426(6)	1.427(5)	1.427	1.421
O1'	C1'	1.322(2)	1.309	1.307	O52	C52	1.375(6)	1.374(5)	1.375	1.345
N7'	C6'	1.398(3)	1.387	1.376	N50	C51	1.431(5)	1.445(6)	1.438	1.424
C1'	C2'	1.407(3)	1.399	1.401	C52	C53	1.403(6)	1.414(7)	1.409	1.401
C2'	C3'	1.380(3)	1.383	1.381	C53	C54	1.395(7)	1.382(6)	1.389	1.384
C3'	C4'	1.411(3)	1.402	1.405	C54	C55	1.400(9)	1.390(8)	1.395	1.394
C4'	C5'	1.376(3)	1.385	1.382	C55	C56	1.378(6)	1.386(7)	1.382	1.385
C5'	C6'	1.401(3)	1.398	1.401	C56	C51	1.397(7)	1.390(6)	1.394	1.393
C6'	C1'	1.400(3)	1.390	1.398	C51	C52	1.390(8)	1.376(8)	1.383	1.397
N7	C8	1.388(2)	1.375	1.369	N43	C44	1.359(5)	1.367(5)	1.363	1.350
N7'	C8'	1.388(2)	1.375	1.369	N50	C49	1.383(5)	1.383(6)	1.383	1.372
C8	C9	1.405(3)	1.396	1.398	C44	C49	1.422(6)	1.442(7)	1.432	1.428
C9	C10	1.378(3)	1.392	1.394	C44	C45	1.412(6)	1.397(6)	1.405	1.407
C10	C10'	1.391(3)	1.396	1.398	C45	C46	1.374(5)	1.372(6)	1.373	1.375
C10'	C9'	1.378(3)	1.381	1.379	C46	C47	1.389(6)	1.397(7)	1.393	1.398
C9'	C8'	1.405(3)	1.381	1.379	C47	C48	1.378(6)	1.374(6)	1.376	1.378
C8'	C8	1.401(3)	1.400	1.407	C48	C49	1.406(5)	1.389(5)	1.398	1.400

A detailed comparison between the X-ray data of **1** and the theoretical results for **1'**-S and **1'**-DR shows a good overall agreement although some differences can also be observed. Most notably, the coordinated dmf molecule is tilted in both optimized structures, which breaks the molecular symmetry of the complex. This behavior is however entirely expected when

considering the observed disorder in the experimental X-ray data. For both **1'**-S and **1'**-DR, the largest deviation between the calculated and experimental bond lengths is about 0.04 Å and all important bond lengths in the complex (including those in *o*-phenylenediamine and *o*-aminophenol rings) are reproduced with good precision (R_{par}[22] values 0.0072 and 0.0045, respectively). The single biggest difference between the structures **1'**-S and **1'**-DR is in the Mo-N bond distances which are about 0.04 Å longer in **1'**-DR and thereby in slightly better agreement with the experimental data. However, the differences in the optimized bond lengths of **1'**-S and **1'**-DR are in general too small in order for any definite conclusions to be drawn about the nature of the electronic ground state of **1**.

The concept of metrical oxidation state (MOS) was introduced recently by Brown[23] and it has been used to quantify the formal oxidation state of non-innocent (oxidized) amidophenoxide or catecholate ligands coordinated to metal ions by examination of their geometrical parameters. The MOS calculated for the experimental structure **1** is 1.55(14). Corresponding values for the DFT optimized structures **1'**-S and **1'**-DR are 1.58(17) and 1.47(15), respectively. From these, the data for **1'**-S is in slightly better agreement with the experimental value although the estimated standard deviations are very high, preventing definite conclusions being made. As explained by Brown, compounds with metal ions in high oxidation state and with two or fewer d electrons, such as molybdenum(VI) and vanadium(V) complexes, tend to have non-integer MOS values which originate from ligand to metal π-donation rather than from an antiferromagnetic coupling of electrons residing in separate orbitals.[23] Considering complex **1**, a visual inspection of frontier MOs of **1'**-S and **1'**-DR shows significant delocalization, which in both cases gives rise to π-bonding between the *o*-phenylenediamine fragment of the ligand and the molybdenum-ion (Figure). This not only explains the similarity in the calculated MOS values for **1'**-S and **1'**-

DR but it also supports the earlier conclusions of the rather small effect that the diradical character has to the overall electronic structure of **1'** (see above).

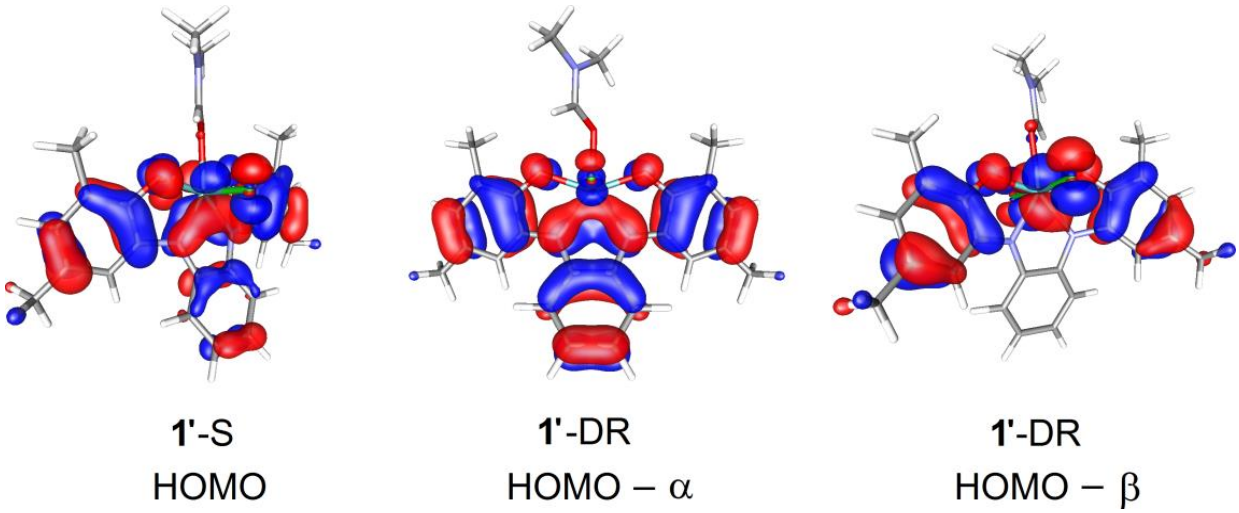

Figure 5. Frontier MOs of **1'**-S and **1'**-DR. The Mulliken populations of the shown orbitals are presented in Supporting Information.

To summarize, although the experimental structural data shows some discrepancies between the expected and observed bond lengths, the results from theoretical calculations indicate that the ground state of **1** is a singlet with a small diradical character, and which cannot therefore be fully described with a closed-shell configuration. The observed deviations in the geometrical parameters of the phenyl rings and Mo-N/O bonds can be attributed primarily to π-donation from the ligand to the high-valent molybdenum cation rather than actual electron transfer creating a lower oxidation state Mo(V) center.

In a similar fashion to **1**, the geometrical parameters of the tridentate ligand in complex **2** suggest some variation in the oxidation state of the ligand which is also evident from the odd number of electrons in this complex. The plausible electronic states for **2** are a doublet (**2'**-D) and a quartet (**2'**-Q). Thus, DFT optimizations were performed to estimate the energy difference

between the two states and the results show the quartet state to be over 80 kJ/mol higher in energy compared to the doublet. It is important to note that a broken symmetry doublet with two unpaired electrons at the ligand and one at the metal center (coupled antiferromagnetically as in **1'**-DR) is also a plausible electronic configuration. However, we were not able to locate a minimum corresponding to such a state; the Mulliken populations in the HOMO (SOMO-1) orbital of **2'**-D have also insignificant (only a few percent) contributions from the metal orbitals, thus excluding the possibility of a broken symmetry type state (see Supporting Information). Hence, the ground state of complex **2** was inferred to be a pure doublet, which is fully supported by the data from magnetometric measurements (see above).

The theoretical model **2'**-D reproduces the experimental geometrical features of **2** from good to excellent precision (R_{par} value for bond distances from Table 1 is 0.0056, excluding the distance between the uncoordinated O52 and Mo1). The calculated data reproduce the key bond lengths around the metal center and show that the Mo-N(radical) bond length is significantly longer (over 0.1 Å) compared with the Mo-N(amido) bond. The structural parameters also show the overall shortening of bonds around the N43 center compared to the amido nitrogen as the latter bonds are about 0.02 to 0.07 Å longer than the former. In addition, small changes in the C-C and C-O bond distances of the neighboring phenyl groups of N43 indicate delocalization of the unpaired electron density over the whole aromatic system. The delocalization is also visible in the calculated spin distribution of **2'** (Figure) which, together with the Mulliken population analysis, shows the unpaired electron to be delocalized over the aromatic rings of the tridentate ligand with roughly one third of the total spin density attributable to the N43 atom.

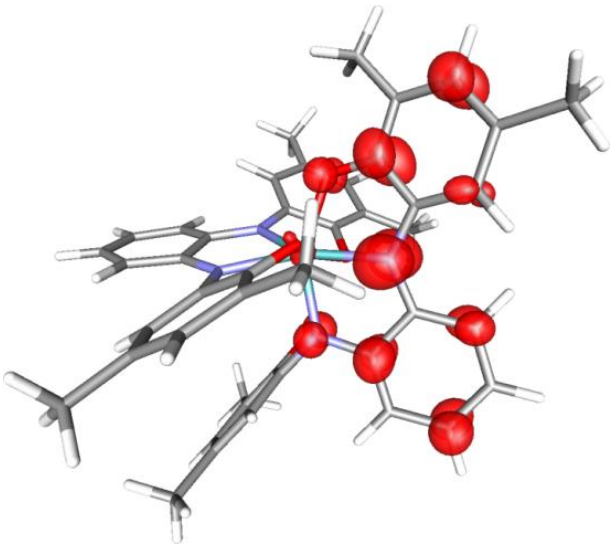

Figure 6. Calculated spin density distribution of complex **2**.

MOSs were calculated for the experimental structure of **2** (two separate molecules in the asymmetric unit) and for the theoretical model **2'**-D. The MOS calculated for **2** from the average experimental bond distances is 1.50(7), whereas the MOSs calculated separately for the individual molecules in the asymmetric unit are 1.42(10) and 1.58(6). The corresponding MOS value for the DFT optimized structure is 1.30(9) which differs slightly from the experimental data although the differences are again within 2σ. These results clearly point out the sensitivity of the MOS analysis to the X-ray data, which prevents an in-depth discussion of the electronic structure of **2**. Similarly to **1**, the calculated non-integer MOSs can be attributed to π-donation from ligand to the high-valent molybdenum cation (with the formal oxidation state Mo(VI)) rather than to any actual ligand to metal electron transfer.

Considered as a whole, the conducted experimental and theoretical investigations present an unambiguous picture of the electronic state and bonding in **2**. To the best of our knowledge, this complex represents the first example of a stable high-valent molybdenum-amidophenoxide radical.

CONCLUSIONS

The redox-active and potentially tetradentate phenolic ligand precursor N,N'-bis(3,5-di-*tert*-butyl-2-hydroxyphenyl)-1,2-phenylenediamine ($H_4N_2O_2$) reacts with $[MoO_2Cl_2(dmf)_2]$ to form a heptacoordinated Mo(VI) complex **1** $[Mo(N_2O_2)Cl_2(dmf)]$ where the tetradentate ligand is fully deprotonated. In contrast, the reaction of the precursor with $[MoO_2(acac)_2]$ leads to the formation of **2** $[Mo(N_2O_2)(HN_2O_2)]$. Both of the prepared complexes present a rare situation of Mo(VI) ion without any multiply bonded terminal ligands. Furthermore, in complex **2**, the non-innocent ligands display both tetradentate and tridentate coordination modes with the latter one containing an unpaired electron and thereby forming the first example of a stable molybdenum-amidophenoxide radical.

EXPERIMENTAL SECTION

Methods and materials. The starting complexes $[MoO_2Cl_2(dmf)_2]$, $[MoO_2(acac)_2]$ and $[MoO_2(Heg)_2]$ were synthesized by literature procedures.[24,25,26] The ligand precursor was prepared and purified according to a published synthesis.[1,3b] Other chemicals were used as purchased from commercial sources. The solvents used were of HPLC grade. All syntheses were done under ambient atmosphere.

ESI-MS for **2** were measured in the positive and negative ion mode Bruker micrOTOF-Q spectrometer. The samples were injected as MeCN-water solutions. Cyclic voltammetry for **2** was recorded at ambient temperature using a platinum working electrode, a 1 mm diameter platinum counter electrode and a Ag/AgCl reference electrode. Samples were dissolved in MeCN containing 0.1 M of $(Bu_4N)ClO_4$ as the supporting electrolyte. The voltammograms were

recorded at a scan rate of 100 mV s^{-1} while the potentials were measured in volts vs. the Fc^{+}/Fc couple.

Solid-state ESR spectra were recorded at 4 K, whereas the solution ESR of **2** (in CH_2Cl_2) was recorded at ambient temperature. The magnetic properties were measured in a SQUID magnetometer with 70 mg and 48 mg samples of **1** and **2**, respectively, sealed in plastic non-magnetic straws. The temperature dependence from 5 to 300 K was measured in a 0.1 T magnetic field using 10 K steps and the field dependence was measured at 5 K between -2 T and 2 T using 50 mT steps. The susceptibility of sample **2** was determined at 5 K from a linear fit to the *M(B)* data.

Preparation of **1**. To a solution of $[MoO_2Cl_2(dmf)_2]$ (173 mg, 0.50 mmol) in acetonitrile (5 ml) was added 260 mg (0.50 mmol) of the ligand precursor dissolved in 10 ml of the same solvent. The resulting intensely dark solution was stored for two days at room temperate to give dark crystals. Crystals were isolated by filtration and washed with 10 ml of ACN to obtain dark green prisms in a 63 % (250 mg) yield. Found: C, 59.25; 7.02; N, 6.80. Calcd for $C_{39}H_{54}Cl_2MoN_4O_3$: C, 59.01; H, 6.86; N, 7.06. IR: 1642 (vs), 1460 (vs), 1377 (s), 1366 (s), 1312 (w), 1289 (w), 1277 (w), 1250 (m), 1189 (w), 1167 (m), 1134 (w), 1111 (w), 1076 (w), 997 (w), 922 (w), 872 (w), 762 (w), 755 (m), 721 (w), 608 (w), 488 (w) cm^{-1}. Complete insolubility of the solid compound prevented further spectroscopic analyses.

Preparation of **2**. A solution of $H_4N_2O_2$ (172 mg, 0.33 mmol) in 10 ml of MeOH was added to a solution of $[MoO_2(acac)_2]$ (55 mg, 0.17 mmol) in 10 ml of the same solvent. A dark bluish color developed rapidly and black shiny crystals were formed during 24 hours at room temperature. The crystals were collected by filtration and washed with 10 ml of methanol to

obtain **2** in a 75 % yield (280 mg). Found: C, 73.42; H, 8.61; N, 5.04. Calcd. for $C_{68}H_{90}MoN_4O_4$: C, 72.70; H, 8.07; N, 4.99. IR: 1460 (vs), 1380 (s), 1362 (s), 1300 (s, br.), 1285 (m), 1260 (m), 1236 (s), 1202 (w), 1130 (m), 1072 (w), 1018 (w), 993 (m), 883 (w), 872 (w), 770 (w), 740 (m), 731 (m), 605 (w), 606 (w) cm^{-1}. 1H NMR ($CDCl_3$) δ: 0.9 -2.1 (72 H, several overlapping peaks), 6.8 – 7.1 (16 H, several broad peaks). ESI(+)-MS: *m*/*z* = 1123.5862 (M^+, calcd 1123.59382); ESI(-)-MS: *m*/*z* = 1123.5915 (M^-, calcd 1123.59382).

X-ray Crystallographic Details. Crystals suitable for single-crystal X-ray measurements were obtained directly from the reaction mixtures. The crystallographic data for compounds **1** and **2** are summarized in

Table **2** along with other experimental details. The data sets were collected at 223 K (**1**) or at 173 K (**2**) with an Enraf Nonius Kappa CCD area-detector diffractometer with the use of graphite monochromated Mo-Kα radiation (λ = 0.71073 Å). Data collection was performed by using φ and ω scans, and the data were processed by using DENZO-SMN v0.93.0[27]. SADABS[28] absorption correction was applied for complex **2**. The structures were solved by direct methods using SHELXS-97[29] and full-matrix least-squares refinements on F^2 were performed using SHELXL-97[29]. All figures were drawn with Diamond 3.[30] For all compounds, the heavy atoms were refined anisotropically, whereas all hydrogen atoms were included at the calculated distances with fixed displacement parameters from their host atoms (1.2 or 1.5 times of the host atom).

Table 2. Summary of crystallographic data for **1** and **2** at 223 K and 173 K, respectively.

	1	**2**
Formula	$C_{39}H_{54}C_{l2}MoN_4O_3$	$C_{68}H_{89}MoN_4O_4$
M_r	793.70	825.74
Crystal system	monoclinic	monoclinic
Space group (no.)	$P2_1/m$ (11)	C2/c (15)
a/Å	9.8327(2)	30.4051(3)
b/Å	18.5416(3)	18.9197(2)
c/Å	11.3473(2)	45.7404(5)
α/°	90.00	90.00
β/°	99.8100(10)	104.2260(10)
δ/°	90.00	90.00
V/Å^3	2036.66(6)	25505.5(5)
Z	2	16
μ(Mo-Kα)/mm^{-1}	0.492	0.254
Obs. reflections	7964	15921
R_{int}	0.0189	0.0226
Parameters	290	1393
R1[a]	0.0405 (0.0314)	0.0808(0.052)
wR2[a]	0.0779 (0.0724)	0.114(0.102)
Goodness of fit	1.057	1.053
Peak, hole */e Å^{-3}*	0.324/-0.435	0.468/-0.372

[a] values in parentheses for reflections with $I > 2.0\sigma(I)$

$R1 = \Sigma \mid |F_o| - |F_c| \mid \; / \; \Sigma |F_o|$

$wR2 = \{ \Sigma [w(F_o^2 - F_c^2)^2] \; / \; \Sigma [w(F_o^2)^2] \}^{1/2}$ and

$w = 1/[\sigma^2(F_o^2) + (aP)^2 + bP)]$, where $P = (2F_c^2 + F_o^2)/3$

Computational Details. All calculations were performed using the Turbomole 6.3 program package.[31] The geometries of the complexes were optimized using the PBE1PBE[19] density functional and Ahlrichs' def2-TZVP[20] basis sets. The nature of stationary points found was assessed by calculating the two lowest eigenvalues of the Hessian matrix. Mulliken population analyses were performed as implemented in the Turbomole 6.3 code. The program gOpenMol[32] was used for visualizations of spin density and molecular orbitals.

ASSOCIATED CONTENT

Supporting Information

Experimental crystallographic information of **1** and **2** in CIF format, as well as optimized structures, data from Mulliken population analyses, and calculated spin densities of **1'** and **2'**. This material is available free of charge via the Internet at http://pubs.acs.org.

AUTHOR INFORMATION

Corresponding Author

* Email: ari.lehtonen@utu.fi; Tel: +358-2-333-6733; Fax: +358-2-333-6700

Notes

The authors declare no competing financial interest.

ACKNOWLEDGMENTS

The authors would like to thank Dr. Pasi Virta for mass spectra and Dr. Pia Damlin for CV measurements. H.M.T. and M.M.H. acknowledge financial support from the Technology Industries of Finland Centennial Foundation. Part of this work was also supported by the COST Action CM1003: "Biological oxidation reactions - mechanisms and design of new catalysts".

REFERENCES

[1] (a) Kaim, W.; Schwederski, B. *Coord. Chem. Rev.* **2010,** *254,* 1580. (b) Kaim, W. *Inorg. Chem.* **2011**, *50*, 9752.

[2] Chauduri, P.; Hess, M.; Müller, J.; Hildenbrand, K. ; Bill, E.; Weyhermüller, T.; Wieghardt, K. *J. Am. Chem. Soc.* **1999**, *121*, 9599.

[3] (a) Blackmore, K. J.; Lal, N.; Ziller, J. W.; Heyduk, A. F. *J. Am. Chem. Soc.*, **2008**, *130*, 2728. (b) Blackmore, K. J.; Lal, N.; Ziller, J. W.; Heyduk, A. F. *Eur. J. Inorg. Chem.* **2009**, 735.

[4] Zelikoff, A. L.; Kopilov, J.; Goldberg, I.; Coates, G. W.; Kol, M. *Chem. Commun.* **2009**, 6804.

[5] Dinda, R.; Sengupta, P.; Ghosh S.; Sheldrick, W.S. *Eur. J. Inorg. Chem.* **2003**, 363.

[6] Pramanik, N.R.; Ghosh, S.; Raychaudhuri, T.K.; Ray, S.; Butcher, R.J.; Mandal, S.S. *Polyhedron* **2004**, 23, 1595.

[7] Mayilmurugan, R.; Harum, B. N.; Volpe, M.; Sax, A. F.; Palaniandavar, M.; Mösch-Zanetti, N. C. *Chem. Eur. J.* **2011**, *17,* 704.

[8] (a) Hanna, T. A; Incarvito, C. D.; Rheingold, A. L. *Inorg. Chem.* **2000**, *39*, 630. (b) Hanna, T. A.; Ghosh, A. K.; Ibarra, C.; Mendez-Rojas, M. A.; Rheingold, A. L.; Watson, W. H. *Inorg. Chem.* **2004**, *43*, 1511. (c) Hanna, T. A.; Ghosh, A. K.; Ibarra, C.; Zakharov, L.; Rheingold, A. L.; Watson, W. H. *Inorg. Chem.* **2004**, *43*, 7567. (d) Liu, L.; Zakharov, L. N.; Golen, J. A.; Rheingold, A. L.; Watson, W. H.; Hanna, T. A. *Inorg. Chem.* **2006**, *45*, 4247.

[9] Lehtonen, A.; Balcar, H.; Sedláček, J.; Sillanpää, R. *J. Organomet. Chem.* **2008**, *693*, 1171.

[10] Kopec,, J. A.; Shekar, S.; Brown, S. N. *Inorg. Chem*. **2012**, *51*, 1239.

[11] Casanova, D.; Alemany, P.; Bofill, J. M.; Alvarez, S. *Chem. Eur. J.* **2003**, *9*, 1281.

[12] Mohn, P. Magnetism in the solid state - an introduction, Springer-Verlag, Berlin, 2003

[13] (a) Ottenwaelder, X; Ruiz-García, R.; Blondin, G.; Carasco, R.; Cano, J.; Lexa, D.; Journaux Y.; Aukauloo, A. *Chem. Commun.***, 2004**, 504. (b) Waldhör, E.; Schwederski, B.; Kaim, W. J. Chem. Soc., *Perkin Trans. 2* **1993**, 2109.

[14] Xiao, Z.; Bruck, M. A.; Doyle, C.; Enemark, J. H.; Grittini, C.; Gable, R. W.; Wedd, A. G.; Young, C. G. *Inorg. Chem.* **1995,** *34***,** 5950

[15] Khusniyarov, M. M.; Harms, K.; Burghaus, O.; Sundermeyer, J.; Sarkar, B.; Kaim, W.; van Slageren, J.; Duboc, C.; Fiedler, J. *Dalton Trans*. **2008**, 1355.

[16] Chaudhuri, P.; Verani, C. N.; Bill, E.; Bothe, E.; Weyhermüller, T.; Wieghardt, K. *J. Am. Chem. Soc.* **2001**, *123*, 2213.

[17] Bhattacharya, S.; Gupta, P.; Basuli, F.; Pierpont, C. G. *Inorg. Chem.* **2002**, *41*, 5810.

[18] (a) Bachler, V.; Olbrich, G.; Neese, F.; Wieghardt K. *Inorg. Chem.* **2002**, *41*, 4179. (b) Das, D.; Sarkar, B.; Mondal, T. K.; Mobin, S. M.; Fiedler, J.; Kaim, W.; Lahiri, G. M. *Inorg. Chem.* **2011**, *50*, 7090. (c) Lu, C. C.; DeBeer George, S.; Weyhermüller, T.; Bill, E.; Bothe, E.; Wieghardt, K. *Angew. Chem., Int. Ed.* **2008**, *47*, 6384. (d) Tomson, N. C.; Labios, L. A.; Weyhermüller, T.; Figueroa, J. S.; Wieghardt, K. *Inorg. Chem.* **2011**, *50*, 5763.

[19] (a) Perdew, J. P.; Burke, K.; Ernzerhof, M. *Phys. Rev. Lett.* **1996**, *77*, 3865. (b) Perdew, J. P.; Burke, K.; Ernzerhof, M. *Phys. Rev. Lett.* **1997**, *78*, 1396. (c) Perdew, J. P.; Ernzerhof, M.;

Burke, K. *J. Chem. Phys.* **1996**, *105*, 9982. (d) Adamo, C.; Barone, V. *J. Chem. Phys.* **1999**, *110*, 6158.

[20] (a) Weigend, F.; Häser, M.; Patzelt, H.; Ahlrichs, R. *Chem. Phys. Lett.* **1998**, *294*, 143. (b) Weigend, F.; Ahlrichs, R. *Phys. Chem. Chem. Phys.* **2005**, *7*, 3297.

[21] Mulliken, R. S., *J. Chem. Phys.* **1955**, *23*, 1833.

[22] R_{par} is defined as $R_{par} = \frac{\Sigma(|P_{exp} - P_{theo}|)}{\Sigma(|P_{exp}|)}$ and can be used to quantitatively measure the fit of theoretical model to experimental one.

[23] Brown, S. N. *Inorg. Chem.* **2012**, *51*, 1251.

[24] Schröder, F.A.; Scherle, J. *Z. Naturfor*. **1973**, *28b*, 46.

[25] Arnaiz, F. J.; Aguado, R.; Sanz-Aparicio, J.; Marinez-Ripoli, M. *Polyhedron* **1994**, *13*, 2745.

[26] Chen, G.J.-J.; McDonald, J.W.; Newton, W.E. *Inorg. Chem.* **1976**, *15*, 2612.

[27] Otwinowski, Z. W. Minor in Methods in Enzymology: Part A (Eds.: C. W. Carter, R. M. Sweet), Academic Press, New York, 1997, vol. 276, pp. 307–326.

[28] Sheldrick, G. M. SADABS, University of Göttingen, Germany, 2002.

[29] Sheldrick, G. M. *Acta Cryst.* **2008**, *A64*, 112.

[30] Diamond - Crystal and Molecular Structure Visualization, Crystal Impact, K. Brandenburg and H. Putz, Postfach 1251, D-53002 Bonn

[31] TURBOMOLE V6.3 2011, a development of University of Karlsruhe and Forschungszentrum Karlsruhe GmbH, 1989-2007, TURBOMOLE GmbH, since 2007; available from http://www.turbomole.com.

[32] (a) Laaksonen, L. *J. Mol. Graphics* **1992**, *10*, 33. (b) Bergman, D. L.; Laaksonen, L.; Laaksonen, A. *J. Mol. Graphics* **1997**, *15*, 301.